Spectroscopy of Nanoscopic Semiconductor Rings

Axel Lorke, R. Johannes Luyken,* Alexander O. Govorov,† and Jörg P. Kotthaus
Sektion Physik und CeNS, LMU München, Geschwister-Scholl-Platz 1, 80539 München, Germany

J. M. Garcia‡ and P. M. Petroff
Materials Department and QUEST, University of California, Santa Barbara, California 93106
(Received 19 August 1999)

Making use of self-assembly techniques, we realize nanoscopic semiconductor quantum rings in which the electronic states are in the true quantum limit. We employ two complementary spectroscopic techniques to investigate both the ground states and the excitations of these rings. Applying a magnetic field perpendicular to the plane of the rings, we find that, when approximately one flux quantum threads the interior of each ring, a change in the ground state from angular momentum $\ell = 0$ to $\ell = -1$ takes place. This ground state transition is revealed both by a drastic modification of the excitation spectrum and by a change in the magnetic-field dispersion of the single-electron charging energy.

PACS numbers: 73.20.Dx, 03.65.Bz, 78.66.Fd

The fascination of ringlike atomic and quantum structures dates back to Kekulé's famous proposal of the structure of benzene [1]. Particularly interesting are the magnetic properties of such nonsimply connected quantum systems, which are related to the possibility of trapping magnetic flux in their interior. Trapping of a single flux quantum in a small molecule such as benzene is impossible with the magnetic fields available in today's laboratories. In recent years, however, the availability of submicron solid-state ring structures has triggered a strong interest in the magnetic properties of rings, especially in view of the fact that, even in the presence of scattering, the many-particle ground state becomes chiral in a magnetic field, which leads to so-called "persistent currents" [2]. The large body of theoretical work on the properties of quantum rings [3] is accompanied by a number of ground breaking experimental investigations of the magnetic and transport properties of rings [4]. These studies have been carried out in the mesoscopic range, where scattering still influences the phase coherent transport, and a large number of quantum states are filled. To the best of our knowledge, no spectroscopic data is available on rings in the scatter-free, few-electron quantum limit. Furthermore, despite a strong theoretical interest [5,6], the only data available on the *excitations* of rings were taken on macroscopic structures [7].

Here, we report on the spectroscopy of the ground states and excitations of self-assembled, nanoscopic InGaAs quantum rings, occupied with one or two electrons each, and subjected to magnetic fields $0 \leq B \leq 12$ T, corresponding to 0–1.5 flux quanta threading the interior of the ring. In both ground state and excitation spectroscopies we observe characteristic changes at about $B = 8$ T which are attributed to the development of a magnetic-field-induced chiral ground state.

The quantum rings are fabricated by solid-source molecular-beam epitaxy, using the Stranski-Krastanov growth mode, which has now become a well-established technique for the fabrication of high-quality, self-assembled semiconductor nanostructures [8]. Recently, we reported on a remarkable change in morphology when InAs self-assembled dots, grown on GaAs, are covered with a thin layer of GaAs and annealed at growth temperature (1 min at 520 °C for the present samples) [9,10]. Then, the shape of the dots drastically changes from that of a lens (roughly 20 nm in diameter, 7 nm in height [11]) to one resembling a volcano, with an increased lateral size (between 60 and 140 nm in *outer* diameter), a reduced height (about 2 nm) and a well-defined center hole of about 20 nm diameter—see also inset in Fig. 1. For the present investigation, these "self-assembled quantum rings" are embedded in a field-effect transistor (FET) structure, which makes it possible to control the number of electrons per ring by application of a suitable bias voltage. The electron number can be monitored by

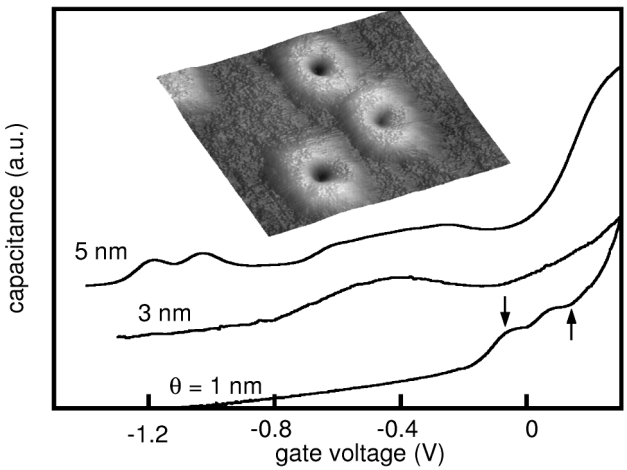

FIG. 1. Capacitance-voltage traces for samples with growth interruption after different coverages of $\theta = 1$, 3, and 5 nm, respectively. The inset displays an atomic force micrograph of self-assembled quantum rings on the surface of a reference sample (scan area: 250×250 nm^2).

capacitance-voltage (*CV*) spectroscopy, which also allows us to derive the many-particle ground state energies of the n-electron system [12,13]. Furthermore, far-infrared (FIR) transmission spectroscopy can be performed simultaneously, to obtain the excitation energies of the electronic system [12,14,15]. It should be pointed out that, even though the fabrication of self-assembled rings has been demonstrated before [9,10], no conclusive evidence was available to show that the surface ring morphology translates into an electronic ring structure inside the completed FET.

The present FET layer sequence starts with a highly Si-doped GaAs backcontact layer and a 25 nm GaAs spacer, followed by the InAs Stranski-Krastanov layer, a 30 nm GaAs cover layer, a 116-nm-thick AlAs/GaAs superlattice, and a 4 nm GaAs cap. Details of the layer sequence and growth procedure, which are essentially identical to those used for quantum dots, can be found in Refs. [11,13]. The crucial step for the ring formation is an interruption in the growth of the GaAs cover layer after the deposition of a nominal thickness θ [9]. On reference samples, which at this stage were removed from the growth chamber, we observe ring formation for θ between 1 and 4 nm. The inset in Fig. 1 shows an atomic force micrograph of a reference sample with $\theta = 2$ nm.

The electronic spectroscopy was performed at liquid He temperatures on samples with an effective area of about 5 mm^2, covering approximately 5×10^8 rings. The *CV* traces were taken at low frequencies (<1 kHz) using the standard lock-in technique; the FIR response was recorded by a rapid-scan Fourier transform spectrometer.

The main part of Fig. 1 displays *CV* spectra of samples with different θ but identical layer sequence. These spectra demonstrate the strong influence that θ has, not only on the morphology of the bare rings [9] but also on the electronic properties inside the completed FET structure. For $\theta = 5$ nm, the spectra are indistinguishable from those of common quantum dot samples without growth interruption [13,14]: We observe a double peak structure at a gate voltage $V_g \approx -1.1$ V, corresponding to the single-electron charging of the two spin states of the so-called "*s* shell" in the dots. Because of inhomogeneous broadening in the present large-area samples, the four maxima of the *p* shell [15] cannot be well distinguished and have merged into a broad plateau at about $V_g \approx -0.4$ V. For details on quantum dot spectroscopy, see, e.g., Refs. [12–15].

For the sample with $\theta = 1$ nm, two peaks can be clearly distinguished at about $V_g \approx 0$ V [16]. For $\theta = 3$ nm, no individual peaks can be identified and only one very broad structure is observed at about $V_g \approx -0.5$ V. We attribute this to the fact that, at the threshold of ring formation, the morphology of the Stranski-Krastanov layer is not well defined. Nevertheless, this data is of significance, as it is a further indication of the structural change that takes place when the growth is interrupted. The shift of the first maximum from -1.2 V ($\theta = 5$ nm) to about 0 V ($\theta = 1$ nm) can be explained by an upward shift of the ground state energy caused by the reduced height of the rings compared to the dots.

In the following, the discussion will focus on the $\theta = 1$ nm ring sample. Figure 2(a) shows the normalized FIR transmission of this sample at $V_g = 0.143$ V (upward arrow in Fig. 1) for two different magnetic fields B, applied perpendicular to the plane of the rings. Comparing the carrier density obtained from either *CV* or FIR spectroscopy with the ring density determined by atomic force microscopy, we find that, at this gate voltage, each ring is filled with approximately $n_e = 2$ electrons, which shows that (as for the dots [13–15]) each *CV* maximum corresponds to the filling of one electron per ring.

It should be pointed out here that the FIR measurements, which require a signal-to-noise ratio of about 1 part in 10^4, are extremely challenging and at the limit of state-of-the-art FIR spectroscopy. However, from a thorough evaluation of a large number of spectra, including subtraction of the superimposed signal from the cyclotron resonance in the backcontact, we can obtain the FIR response as a function of the magnetic field, which is shown in Fig. 2(b).

As indicated by the different symbols, the resonances in Fig. 2(b) can be grouped into the following modes: two resonances (∘) which are degenerate at $B = 0$ and exhibit orbital Zeeman splitting when a magnetic field is applied and a low-lying mode (◇) which, due to an insufficient

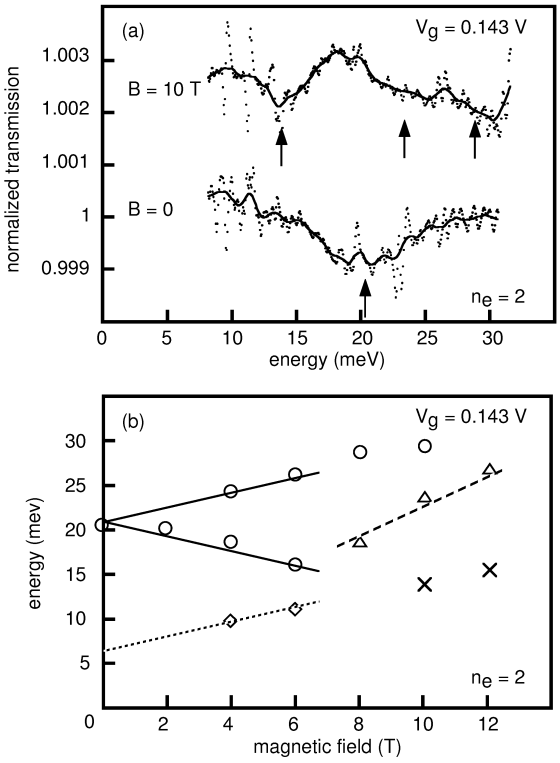

FIG. 2. (a) Normalized transmission of self-assembled quantum rings (filled with $n_e = 2$ electrons each) at magnetic fields $B = 0$ and $B = 10$ T. Minima in the transmission (arrows) correspond to electronic excitations. The solid lines are a smoothed representation of the data points. Curves are offset for clarity. (b) Resonance positions as a function of the magnetic field.

signal-to-noise ratio at very low energies, can only be detected above 10 meV, but extrapolates to ≈7 meV at $B = 0$. This mode dies out at about $B = 7$ T, when also the lower ∘ mode vanishes and a new mode (△) appears. The resonances summarized in Fig. 2(b) differ quite strongly from those observed in quantum dots [14,17], where in general, only two resonances are observed, one of which increases with increasing field, whereas the other decreases. On the other hand, Fig. 2(b) can be directly compared to the excitation spectrum of quantum rings, as calculated, e.g., by Halonen *et al.* [18]. Even though these calculations were performed for a ring with much larger dimensions, all of the above experimental features are in good qualitative agreement with the calculated energy dispersion. Furthermore, using the effective mass of $m^* \approx 0.07 m_e$ found in other self-assembled In(Ga)As quantum structures [12,14,15], we find that the slopes of the ∘ modes ($\pm\frac{1}{2}\hbar\omega_c$, solid lines), the ◇ mode ($\frac{1}{2}\hbar\omega_c$, dotted line), and the △ mode ($\hbar\omega_c$, dashed line) are all in agreement with the calculations. From this we conclude that indeed the morphology seen in Fig. 1 is preserved when the growth is continued, and that it translates into a ringlike electronic structure. As will be discussed in the following, the change in the spectrum at about $B = 8$ T can then be understood as a direct consequence of a magnetic-field-induced change in the ground state. The × mode is not found in the calculated ring excitations of Ref. [18]. At present, an explanation for these resonances is still missing, and it cannot be ruled out that these resonances originate from the presence of a few large quantum dots which have not developed into rings and therefore do not change their ground state at $B = 8$ T.

The electronic states in rings can be discussed using a simple model of a circular, one-dimensional wire, bent into a circle of radius R. The energy levels then follow from the periodic boundary conditions to $E_\ell = \frac{\hbar^2}{2m^*} k_\ell^2$ with $k_\ell = \ell \frac{1}{R}$. When a flux $\phi = \pi R^2 B$ penetrates the interior of the ring, an additional phase is picked up by the electron on its way around the ring, which leads to [3]

$$E_\ell = \frac{\hbar^2}{2m^* R^2}\left(\ell + \frac{\phi}{\phi_0}\right)^2, \quad \ell = 0, \pm 1, \pm 2, \ldots, \quad (1)$$

with ϕ_0 being the flux quantum. Thus, with increasing magnetic field, the ground state will change from angular momentum $\ell = 0$ to one with higher and higher negative ℓ [see Fig. 3(a)], a fact intimately related to the persistent currents in mesoscopic rings [2,3]. Furthermore, a periodic, Aharonov-Bohm–type oscillation in the ground state energy will take place [3], as shown in Fig. 3(a). Obviously, each change in the ground state will in turn lead to a pronounced change in the possible transitions, such as the one seen in Fig. 2(b) at $B \approx 8$ T.

For a more quantitative description of the energies and transitions in the present rings, we have used a model by Chakraborty *et al.* [3,18] and calculated the single-particle states in a ring potential $U(r) = \frac{1}{2} m^* \omega_0^2 (r - R_0)^2$ [see inset in Fig. 3(b)], where ω_0 is the characteristic frequency of the radial confinement and R_0 is the radius of the ring. These two parameters determine the low energy resonance at $B = 0$, estimated at about 7 meV and corresponding to an azimuthal excitation $\Delta\ell = \pm 1, \Delta N = 0$, as well as the high energy resonance at 20 meV, corresponding to an excitation $\Delta\ell = \pm 1, \Delta N = 1$, where N is the radial quantum number. In this way, both parameters are readily determined to be $R_0 = 14$ nm and $\hbar\omega_0 = 12$ meV. The electronic radius of 14 nm is in good agreement with the effective radius of the uncovered rings (i.e., the radius where the InGaAs has maximum thickness, see Fig. 1), which is roughly 18 nm. Furthermore, we find satisfactory agreement between the calculated and measured transitions over the entire range of magnetic fields.

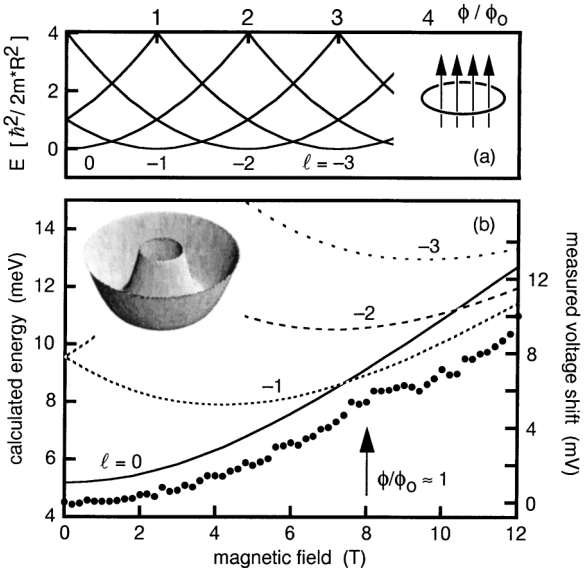

FIG. 3. (a) Energy levels of an ideal one-dimensional ring as a function of the magnetic flux ϕ threading the ring area. (b) Calculated energy levels in a parabolic wire bent into a circular ring (see inset). The data points (right-hand scale) give the gate-voltage shift of the lowest capacitance maximum.

The lines in Fig. 3(b) represent the magnetic-field dispersion of the ring energy levels, calculated with the above values for R_0 and ω_0. The calculations predict a ground state transition (arrow) from $\ell = 0$ to $\ell = -1$ at $B \approx 8$ T, in good agreement with the position of the change in the FIR resonances. This agreement is somewhat surprising, considering that the FIR data was obtained for $n_e = 2$, whereas the model is single particle. From this we conclude that (as in self-assembled InAs dots [14,19]) the single-particle states are a quite accurate basis for the description of the many-particle states and excitations. This is supported by the fact that the measured FIR resonance positions for $n_e = 1$ are very similar to those for $n_e = 2$, even though the signal-to-noise ratio for $n_e = 1$ does not allow us to clearly identify all resonances shown in Fig. 2(b).

There is an additional way to confirm the ground state transition associated with the trapping of flux inside the

rings. By carefully evaluating the position of the lowest capacitance maximum (downward arrow in Fig. 1), we have a direct experimental access to the $n_e = 1$ ground state energy. The data points in Fig. 3(b) summarize the shift in gate voltage of the lowest capacitance peak as a function of the magnetic field. As indicated by the arrow, at $B = 8.2$ T, corresponding to a flux of $\pi R_0^2 B \approx \phi_0$, a change in the slope can be identified in the data which is attributed to the magnetic-field-induced ground state transition from $\ell = 0$ to $\ell = -1$.

Note that the shift of the $n_e = 1$ charging peak is given in mV [right-hand scale in Fig. 3(b)]. From a comparison with the calculations (left-hand scale) we find a voltage-to-energy conversion factor of $f = e\Delta V_g/\Delta E = 1.8$. Using the lever arm model [20], which is quite accurate in the case of quantum dots [13,14,19], the present layer structure gives $f = 7$. We attribute this discrepancy to the fact that the slopes at which the $\ell = 0$ and $\ell = -1$ states intersect strongly depend on the detailed choice of the confining potential [as can readily be seen from a comparison between Figs. 3(a) and 3(b)]. This sensitivity could in fact provide a useful handle to derive the confining potential from more elaborate model calculations.

Converting the separation between the lowest charging peaks in Fig. 1 into energy, we obtain a Coulomb interaction energy of roughly 20 meV for both rings and dots. This similarity is somewhat surprising, given the larger lateral size of the rings. The missing central part, which will decrease the effective area, may partly be responsible for the large Coulomb interaction in the rings.

In summary, we have used the striking morphological change that takes place when self-assembled InAs quantum dots are partially covered with GaAs to fabricate nanoscopic quantum rings with dimensions that bridge the size range between mesoscopic and molecular ring structures [21]. The electron states in these rings are not affected by the presence of random scatterers and are dominated by quantum effects rather than Coulomb interaction. We have identified a magnetic-field-induced transition from a ground state with zero angular momentum to a chiral ground state. This transition is a direct consequence of the nonsimply connected ring geometry [22] and takes place when approximately one flux quantum penetrates the effective interior area of the rings.

We would like to thank R. J. Warburton, K. Karraï, T. Chakraborty, V. Gudmundsson, and M. Barranco for helpful and inspiring comments, the latter also for making their unpublished work available to us. Financial support from QUEST, a NSF Science and Technology Center, from BMBF, through Grant No. 01 BM 623, a Max Planck research award, and the Volkswagen-Stiftung is gratefully acknowledged.

*New address: Infineon Technologies, Otto Hahn Ring 6, 81739, München.

†Permanent address: Institute of Semiconductor Physics, 630090 Novosibirsk-90, Russia.

‡New address: Instituto de Microelectrónica de Madrid, Isaac Newton 8, 28760 Tres Cantos, Madrid, Spain.

[1] A. Kekulé, Bull. Soc. Chim. Fr. **3**, 98 (1865).
[2] M. Büttiker, Y. Imry, and R. Landauer, Phys. Lett. **96A**, 365 (1983).
[3] For reviews, see, e.g., A. G. Aronov and Yu. V. Sharvin, Rev. Mod. Phys. **59**, 755 (1987); T. Chakraborty and P. Pietiläinen, Phys. Rev. B **50**, 8460 (1994); L. Wendler and V. M. Fomin, Phys. Status Solidi (b) **191**, 409 (1995); references therein.
[4] L. P. Lévy *et al.*, Phys. Rev. Lett. **64**, 2074 (1990); V. Chandrasekhar *et al., ibid.* **67**, 3578 (1991); D. Mailly, C. Chapelier, and M. Benoit, *ibid.* **70**, 2020 (1993); A. F. Morpurgo *et al., ibid.* **80**, 1050 (1998); R. Schuster *et al.*, Nature (London) **385**, 417 (1997).
[5] A. Emperador *et al.*, Phys. Rev. B **59**, 15 301 (1999); I. Magnúsdóttir and V. Gudmundsson, http://xxx.lanl.gov/abs/cond-mat/9907216, and references therein.
[6] L. Wendler *et al.*, Phys. Rev. B **54**, 4794 (1996).
[7] C. Dahl *et al.*, Phys. Rev. B **48**, 15 480 (1993).
[8] L. Landin *et al.*, Science **280**, 262 (1998), and references therein.
[9] J. M. García *et al.*, Appl. Phys. Lett. **71**, 2014 (1997).
[10] A. Lorke and R. J. Luyken, Physica (Amsterdam) **256B**, 424 (1998).
[11] D. Leonard *et al.*, Appl. Phys. Lett. **63**, 3203 (1993).
[12] H. Drexler *et al.*, Phys. Rev. Lett. **73**, 2252 (1994).
[13] G. Medeiros-Ribeiro, D. Leonard, and P. M. Petroff, Appl. Phys. Lett. **66**, 1767 (1995).
[14] M. Fricke *et al.*, Europhys. Lett. **36**, 197 (1996).
[15] B. T. Miller *et al.*, Phys. Rev. B **56**, 6764 (1997).
[16] On some samples, a third maximum at $V_g \approx 0.2$ V can be identified [H. Pettersson *et al.*, Report No. Proc. EP2DS13 (to be published)].
[17] C. Sikorski and U. Merkt, Phys. Rev. Lett. **62**, 2164 (1989); T. Demel *et al.*, Phys. Rev. Lett. **64**, 788 (1990).
[18] V. Halonen, P. Pietiläinen, and T. Chakraborty, Europhys. Lett. **33**, 377 (1996).
[19] R. J. Warburton *et al.*, Phys. Rev. B **58**, 16 221 (1998).
[20] This model assumes a linear voltage drop between the backcontact and the front gate, so that the voltage-to-energy conversion factor is simply given by $ed_{\mathrm{In}}/d_{\mathrm{top}}$, where d_{In} and d_{top} are the distances between the back contact and the InGaAs layer/top gate, respectively. For a theoretical assessment of this model, see, e.g., O. Heller, Ph. Lelong, and G. Bastard, Physica (Amsterdam) **249B**, 271 (1998).
[21] Carbon nanotubes are topologically related systems in a similar size range. The magnetotransport properties of carbon nanotubes have been studied, e.g., by A. Bachtold *et al.*, Nature (London) **397**, 6721 (1999).
[22] It is interesting to note that for the discussed ground state transition, the nonsimply connected geometry is a strict requirement only for *normal-metallic* systems. In *superconducting* systems, on the contrary, Aharonov-Bohm–type oscillations can also be observed in a disk geometry [V. V. Moshchalkov *et al.*, Nature (London) **373**, 319 (1995)]. This difference is rooted in the subtleties of the boundary conditions, as discussed in R. Benoist and W. Zwerger, Z. Phys. B **103**, 377 (1997).